PHYSICAL REVIEW B VOLUME 15, NUMBER 12 15 JUNE 1977

Electric-field-gradient tensor in nonmagnetic dilute alloys of copper

Paul L. Sagalyn and Michael N. Alexander
Army Materials and Mechanics Research Center, Watertown, Massachusetts 02172
(Received 17 November 1976)

Calculations are presented for the electric-field gradient q, the asymmetry parameter η, and the direction of the main principal axis of the electric-field-gradient (EFG) tensor, at nearest neighbors (1NN) and second neighbors (2NN) to isolated Zn, Ga, Ge, Ag, Cd, In, Sn, and Sb impurities in copper. A "size effect" contribution, proportional to the local strain about the impurity, is added in tensor fashion to the well-known "valence effect" EFG calculated by Kohn and Vosko and Blandin and Friedel. When the point-charge model is used to evaluate the size-effect EFG tensor, a nonzero asymmetry parameter becomes possible. The calculation also includes an explicit evaluation of the contribution to the EFG of the screening charge which is outside the atomic cell of the host atom being resonated. At the 1NN and 2NN sites the resulting correction to the valence-effect calculation can be as large as 40%; asymptotically, the correction is 17% (assuming $\alpha = 23.3$ for the Kohn-Vosko enhancement factor). When the valence and size effects are combined, good agreement between theory and experiment is obtained. Experimental q's at the 2NN sites in all alloys studied are accounted for by using the parameters $\alpha = 18$, $\lambda = -15$, where α is the Kohn-Vosko enhancement parameter and λ is the EFG-strain coupling constant. These parameters also account well for q and η at the 1NN in alloys with the 5th-row impurities Ag, Cd, In, Sn, and Sb, but the optimal fit for the 1NN is with $\alpha = 15$, $\lambda = -18$. The 1NN data for alloys with the 4th-row impurities Zn, Ga, and Ge can be fit with $\alpha = 2$, $\lambda = 87$, but for no other range of the parameters. The reasons for such different values of α and λ are not understood. However, the resulting fit for the 1NN q and η is excellent, and the "anomalous" direction of the main principal axis in *Cu*Ge is correctly predicted.

I. INTRODUCTION

This paper deals with the interpretation of measurements of the components of the electric-field-gradient (EFG) tensor in nonmagnetic dilute alloys of copper.

Since the pioneering research of Bloembergen and Rowland,[1] extensive NMR work has been carried out on a wide variety of alloy systems. Copper has been a "classic" host because it is cubic, monovalent, and is for many purposes describable by the nearly-free-electron model. Moreover, a large number of impurities dissolve in it.

The early NMR work, which was entirely on powdered samples, demonstrated the existence of what at the time were considered surprisingly large electric field gradients in the vicinity of isolated impurity atoms in dilute alloys. These EFG's, by coupling to the Cu nuclear quadrupole moment, caused sharp reductions in the NMR intensity.

The "wipe out" numbers deduced from such NMR experiments[2] appeared to be dominated by the difference in valence between the host and impurity. Kohn and Vosko[3] (KV), and Blandin and Friedel[4] were able to account semiquantitatively for the experimental wipeout numbers by calculating the EFG produced by the long-range oscillatory screening charge cloud which surrounds the impurity atom. We shall refer to this as the "valence effect."

Sagalyn, Paskin, and Harrison[5] (SPH), using a phenomenological approach, showed that variations in wipe-out number between copper-based alloys containing impurities of the *same* valence could be accounted for by combining the valence effect with an EFG due to the difference in size between host and impurity atoms ("size effect"). However, the magnitude of the EFG-strain coupling constant λ required to account for the alloy data was much larger than the constant inferred from experiments on plastically deformed pure copper.[6-10]

In the early experiments it was not possible to measure the change in Knight shift caused by dilute alloying, since copper atoms near the isolated impurities were wiped out of the observable NMR line.

The use of higher magnetic fields, higher-sensitivity NMR spectrometers—and especially the use of single-crystal techniques[11]—has resulted in considerably more detailed data on dilute copper-based alloys. The Knight shift, and both the magnitude of the EFG and the asymmetry parameter, have been measured for host copper atoms which are near neighbors to a variety of impurities.[12-17]

The recent measurements of the EFG tensor at nearest neighbors (1NN) and next-nearest neighbors (2NN) to isolated impurities are in striking disagreement with results based on valence-effect theories.[13-16] The magnitudes of the experimental

EFG's at the 1NN and 2NN sites are much larger than predicted by the best valence-effect calculations available. Even more striking is the complete failure of the simple valence-effect theory to account for the lack of cylindrical symmetry of the EFG at the 1NN site. The asymmetry parameter η describes the deviation from cylindrical symmetry. From the definition of η it follows that $0 \leq \eta \leq 1$, and that $\eta = 0$ if the EFG tensor has cylindrical symmetry.[18] It has been found experimentally that at 1NN sites η varies from 0.036 (for *Cu*Cd) to 0.905 (for *Cu*Ge— a variation over virtually the entire allowed range). The valence-effect theory, however, predicts that $\eta = 0$ for *all* impurities!

A more sophisticated valence-effect theory, taking into account such factors as asphericity of the host Fermi surface and dielectric tensor, might, it is true, predict a nonzero asymmetry parameter. However, it is difficult to see how any effect which depends primarily on the electronic structure of the host could account for the strong impurity dependence of η. Furthermore, since η is by definition a ratio of components of the EFG tensor, it should be independent of effects which scale simply with the difference in valence between the impurity and host.

Moreover, in certain cases a very large asphericity of the screening charge would be required to explain the experimental results. A spherical screening charge leads to an EFG with the component of largest magnitude q in the direction of the vector $\vec{R}$ which connects the impurity and the host atom which is being resonated (cf. Fig. 3), and with $\eta = 0$. Since the EFG tensor is traceless, its component along the x axis of the crystal must be $-\frac{1}{2}q$. However, it is known experimentally that in *Cu*Ge and *Cu*Si the largest component of the tensor for 1NN Cu atoms is in the direction of the x axis[13-16] Thus, in a screening theory, the distortion of the charge cloud would have to be large enough to change the ratio of the x and R components of the EFG by more than a factor of 2.

We account for the new NMR results on the EFG tensor by use of a model which combines the valence effect and the size effect in a manner similar to, but more general than, that of SPH. SPH assumed an isotropy condition for the EFG-strain coupling tensor F_{ij}. The isotropy condition results in a size-effect EFG whose Principal Axis coincides with the Principal Axis of the valence-effect EFG and for which $\eta = 0$. This makes it possible simply to add the Principal Values for the two effects as scalars. In Sec. III we drop the isotropy condition in favor of the point-charge model, and show this leads to a nonzero asymmetry parameter for the size effect at the 1NN site.

The large discrepancy between the theoretical and experimental magnitudes of the EFG also prompted us to reexamine the valence effect. In the original valence-effect calculation[3] it was estimated the screening charge outside the atomic sphere of the host atom under consideration contributes only 10% to the EFG at large distances from the impurity. In Sec. II we show that at the near neighbors to the impurity, contributions from outside the atomic sphere have the same order of magnitude as contributions from screening charge inside the atomic sphere.

In Sec. IV we combine the valence-effect and size-effect contributions to the EFG tensor, and in Sec. V we compare numerical results with experimental data. Further discussion of the results occurs in Sec. VI, and conclusions are summarized in Sec. VII.

II. THEORY OF THE VALENCE EFFECT

The geometry for the calculation of the valence effect is shown in Fig. 1. Consider a copper (host) atom at a distance R from an impurity atom having an excess valence Z_{eff}. We define a "host sphere" having radius $\frac{1}{2}d$ and centered at the copper atom, where d is the nearest-neighbor distance in the pure material. The "impurity sphere" is then a sphere of radius $R - \frac{1}{2}d$. The outer sphere shown in Fig. 1 is centered at the impurity atom, and has radius $R + \frac{1}{2}d$.

Since we will consider only screening charge distributions which have spherical symmetry with respect to the impurity, the screening charge outside the sphere of radius $R + \frac{1}{2}d$ does not contribute to EFG's at points inside that sphere. For

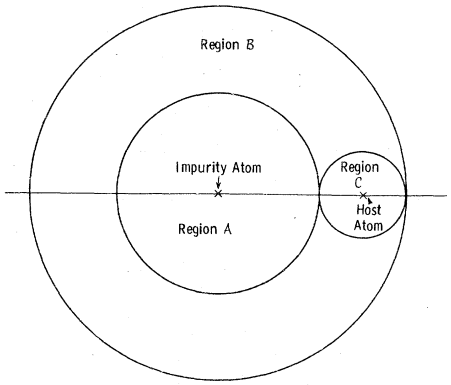

FIG. 1. Geometry used in calculation of valence-effect EFG. Spherical coordinates centered at the impurity atom are labeled $r\theta\Phi$, and spherical coordinates centered at the host atom are labeled $r'\,\theta'\,\Phi'$. The host-impurity separation is denoted by R.

the calculation of the EFG we shall call the impurity sphere region $\mathfrak{A}$, the host sphere region $\mathfrak{C}$, and the remaining volume within the outer sphere region $\mathfrak{B}$.

The EFG tensor q_{ij} has three principal values. When the magnitudes of the principal values are known we will follow the usual custom of labeling the principal axes X, Y, Z in such a way that $|q_{ZZ}| \geq |q_{YY}| \geq |q_{XX}|$.[18] To avoid confusion with the literature, we will follow custom and refer to q_{ZZ} as "the electric field gradient," written simply as q (when referring to the ensemble of components we may add the work "tensor" for clarity). We will also refer to q_{ZZ} as the Principal Value (with capital letters) of the EFG.

The Z axis for the total valence-effect EFG resulting from regions $\mathfrak{A}$, $\mathfrak{B}$, and $\mathfrak{C}$ will be parallel to the vector $\vec{R}$ connecting the impurity atom to the host atom at which the EFG is being calculated. We employ the notation $q_{\parallel}^{V} \equiv q_{ZZ}^{V}$ to emphasize this fact, which is important when the valence and strain effects are combined (Sec. IV).

A. Region $\mathfrak{C}$

The portion of $q_{\parallel}^{V}$ contributed by region $\mathfrak{C}$, and which we denote $q_{\parallel}^{\mathfrak{C}}$, has been calculated by Jensen, Nevald, and Williams.[14] The result is[19]

$$q_{\parallel}^{\mathfrak{C}} = \alpha 4\pi k_F^3 \left(\frac{\frac{2}{3}A\cos(2k_FR+\phi)}{(k_FR)^3} + \frac{\frac{2}{3}k_FB\cos(2k_FR+\xi) - A\sin(2k_FR+\phi)}{(k_FR)^4} \right), \tag{1}$$

where k_F is the Fermi wave vector and α is the enhancement factor, which results from antishielding within the host atom.[3] The term with R^{-3} was derived by KV[3] and by Blandin and Friedel.[4] The terms with R^{-4} were derived by adding the Alfred–Van Ostenburg preasymptotic screening charge term[20] to the asymptotic screening. Expressions are given in Ref. 14, from which the coefficients A, B and the phase constants ϕ, ξ may be determined in terms of scattering phase shifts.[19]

KV obtained the value $\alpha = 23.3$ for region $\mathfrak{C}$ alone. The commonly quoted value $\alpha = 25.6$ includes KV's estimate of the 10% contribution from charges outside the host atom sphere.

The asymptotic form of Eq. (1) is

$$q_{\parallel}^{\mathfrak{C}} \sim \tfrac{64}{3}\pi k_F^3 \alpha A \cos(2k_FR+\phi)/(2k_FR)^3 \quad (R \to \infty). \tag{2}$$

B. Region $\mathfrak{A}$

The component of the EFG along the $\vec{R}$ direction produced by the charge in region $\mathfrak{A}$ is

$$q_{\parallel}^{\mathfrak{A}} = -(1/e)2\mathfrak{Q}(1-\gamma_\infty)/R^3, \tag{3}$$

where $\mathfrak{Q}$ is the net charge in region $\mathfrak{A}$, γ_∞ is the Sternheimer antishielding constant,[21] and e is the charge of the electron.

If the excess charge on the impurity were not screened, the EFG at the 1NN site would numerically be about $2Z_{\text{eff}}$ Å^{-3} (since $R \simeq 2.56$ Å, $R^3 \simeq 1-\gamma_\infty$ Å^3). This is much larger than the experimentally observed values. Until now it has been assumed that the impurity atom is completely screened in a distance of the order of the 1NN distance, and that the contribution of region $\mathfrak{A}$ to the EFG can be neglected.[10] We shall here explicitly calculate its contribution.

The net charge within region $\mathfrak{A}$ is

$$\mathfrak{Q} = Z_{\text{eff}}\, e + e\int_0^{R-d/2} \Delta n(\vec{r})\, d^3r, \tag{4}$$

where $e\Delta n(\vec{r})$ is the screening charge distribution. The condition of overall charge neutrality is

$$Z_{\text{eff}} = -\int_0^{\infty} \Delta n(\vec{r})\, d^3r. \tag{5}$$

Therefore,

$$\mathfrak{Q} = -e\int_{R-d/2}^{\infty} \Delta n(\vec{r})\, d^3r. \tag{6}$$

Since the integral in Eq. (6) excludes the origin, we can use for $\Delta n(r)$ the form given by Alfred and Van Ostenburg[20]

$$-\Delta n(r) \simeq A\cos(2k_Fr+\phi)/r^3 + B\cos(2k_Fr+\xi)/r^4, \tag{7}$$

where the coefficients and phase constants are the same as those in Eq. (1). We have, finally,

$$\mathfrak{Q} \simeq -4\pi e\int_{R-d/2}^{\infty} r^2\Delta n(r)\, dr \equiv -(I+J). \tag{8}$$

I and J are given by

$$I = 4\pi eA\{-\cos\phi\,\mathrm{Ci}(2k_FR') + \sin\phi[\mathrm{Si}(2k_FR') - \tfrac{1}{2}\pi]\},$$

$$J = 8\pi eBk_F\{\cos\xi[(2k_FR')^{-1}\cos(2k_FR') + \mathrm{Si}(2k_FR') - \tfrac{1}{2}\pi] - \sin\xi[(2k_FR')^{-1}\sin(2k_FR') - \mathrm{Ci}(2k_FR')]\}, \tag{9}$$

where $\mathrm{Si}(x)$ and $\mathrm{Ci}(x)$ are the sine and cosine integrals, defined by

$$\mathrm{Si}(x) = \int_0^x t^{-1}\sin t\, dt$$

and

TABLE I. Contribution of valence effect to 1NN EFG in dilute alloys of copper. EFG's, unless otherwise noted, are evaluated at positions to which 1NN atoms are displaced by the impurity, as given by d_1 in column 2 (with no displacement, d_1=4.830 a.u.). EFG's are in units of 10^{24} cm^{-3}.

Impurity	d_1 (a.u.)	EFG Region 𝔄	EFG Region 𝔅	EFG Region ℭ (α=15)	Total valence-effect EFG 𝔄+𝔅+ℭ	Total valence-effect EFG 𝔄+𝔅+ℭ No strain
Zn	4.861	0.086	−0.076	−0.051	−0.042	−0.038
Ga	4.872	0.048	−0.102	−0.159	−0.213	−0.214
Ge	4.882	0.048	−0.254	−0.454	−0.660	−0.681
Ag	4.918	−0.068	0.062	0.044	0.038	0.034
Cd	4.954	0.090	−0.083	−0.048	−0.041	−0.029
In	4.977	0.141	−0.171	−0.164	−0.194	−0.176
Sn	4.988	0.052	−0.194	−0.336	−0.479	−0.512
Sb	4.999	−0.097	−0.227	−0.564	−0.888	−1.036

$$\mathrm{Ci}(x) = -\int_x^\infty t^{-1}\cos t\,dt.$$

I represents the integration over the term in Eq. (7) that goes as r^{-3}, J represents the integration over the term that goes as r^{-4}, and $R' \equiv R - \frac{1}{2}d$.

To find an asymptotic form for $\mathfrak{L}$, we use the expressions[22]

$$\begin{aligned}&\mathrm{Ci}(x) \longrightarrow x^{-1}\sin x - x^{-2}\cos x\,,\\ &\mathrm{Si}(x) \longrightarrow -x^{-1}\cos x - x^{-2}\sin x + \tfrac{1}{2}\pi \qquad (x\to\infty)\,.\end{aligned} \tag{10}$$

Substituting Eq. (10) into Eqs. (8) and (9), we find that as $R\to\infty$

$$\mathfrak{L} \longrightarrow 4\pi eA(2k_FR)^{-1}\sin(2k_FR+\phi-k_Fd)\,. \tag{11}$$

From this, it can be seen that the screening charge surrounding the impurity decreases only as R^{-1}. This shows that, in contrast to what is often assumed, screening of the impurity is a very long-range phenomenon.[23]

Using Eq. (11) in Eq. (3) we find that for large R the form of $q_\parallel^{\mathfrak{A}}$ is

$$q_\parallel^{\mathfrak{A}} \sim -64\pi Ak_F^3(1-\gamma_\infty) \times \sin(2k_FR+\phi-k_Fd)/(2k_FR)^4\,. \tag{12}$$

Equation (12) can be compared with the asymptotic form for the EFG from region ℭ, given in Eq. (2). The ratio $|q_\parallel^{\mathfrak{A}}/q_\parallel^{\mathfrak{C}}|$ is $[(1-\gamma_\infty)/\alpha](3/2k_FR)$. Using k_F = 0.719 a.u., γ_∞ = −17.36, and α = 23.3, we find that for the ratio to be less than 10%, R must be greater than 16 a.u., or beyond the 11th neighbor to the impurity. Thus region 𝔄 cannot be neglected even for the longer distances used in wipe-out calculations.

C. Region 𝔅

For region 𝔅 we use the general expression for the EFG at the host site

$$q_\parallel^{\mathfrak{B}} = \int r'^{-3}\Delta n(\vec{\mathfrak{r}}')(3\cos^2\theta'-1)(1-\gamma_\infty)\,d^3r'\,, \tag{13}$$

where

$$d^3r' = r'^2\sin\theta'\,dr'\,d\theta'\,d\Phi'$$

is expressed in coordinates centered at the host atom. It is convenient to evaluate this using a coordinate system centered at the impurity (c.f., Fig. 1), and therefore make the substitution

$$r = (R^2 + r'^2 + 2r'R\cos\theta')^{1/2}.$$

The resulting formula is complicated and will not be reproduced here. The contribution from region 𝔅 was evaluated numerically. Convergence tests indicate that the accuracy of the results (Tables I and II) is better than 2%.

Our derivation of an asymptotic form for $q_\parallel^{\mathfrak{B}}$ is given in Appendix A. To lowest order in $1/R$ we find [see Eq. (A10)]

$$q_\parallel^{\mathfrak{B}} \sim 64\pi Ak_F^3(1-\gamma_\infty) \times\left(\frac{\sin k_Fd}{(k_Fd)^3} - \frac{\cos k_Fd}{(k_Fd)^2}\right)\frac{\cos(2k_FR+\phi)}{(2k_FR)^3}\,.$$

Using α = 23.3, $d = 2.556\times10^{-8}$ cm, and the values of k_F and γ_∞ given in Sec. II B, we find that as $R\to\infty$

$$q_\parallel^{\mathfrak{B}}/q_\parallel^{\mathfrak{C}} \sim 0.167\,.$$

Thus the valence-effect EFG contributions from regions 𝔅 and ℭ have the same asymptotic form and the same phase. When α = 23.3, the contribution of region 𝔅 is about 17%, in rough agreement with the estimate by KV that the screening charge outside the host atom enhances the EFG due to region ℭ by about 10%. Note, however, that the fractional correction brought about by inclusion of region 𝔅—and region 𝔄, also, when R is not large—depends on the value of the en-

TABLE II. Contribution of valence effect to 2NN EFG in dilute alloys of copper. EFG's, unless otherwise noted, are evaluated at positions to which 2NN atoms are displaced by the impurity, as given by d_2 in column 2 (with no displacement, $d_2 = 6.8308$ a.u.). EFG's are in units of 10^{24} cm^{-3}.

Impurity	d_2 (a.u.)	EFG Region 𝔄	EFG Region 𝔅	EFG Region ℭ ($\alpha = 18$)	Total valence-effect EFG 𝔄 + 𝔅 + ℭ	Total valence-effect EFG 𝔄 + 𝔅 + ℭ No strain
Zn	6.846	−0.012	0.007	0.004	−0.001	−0.002
Ga	6.852	−0.020	0.021	0.037	0.038	0.036
Ge	6.857	−0.048	0.072	0.149	0.173	0.171
Ag	6.875	0.010	−0.010	−0.015	−0.015	−0.015
Cd	6.893	−0.012	0.010	0.008	0.006	0.004
In	6.904	−0.028	0.026	0.032	0.029	0.023
Sn	6.910	−0.041	0.055	0.107	0.121	0.114
Sb	6.915	−0.054	0.105	0.240	0.290	0.290

hancement factor α. If $\alpha < 23.3$, as we find in our analyses of data in Sec. V below, the relative importance of regions 𝔄 and 𝔅 increases.

D. Total valence-effect EFG

The results for regions 𝔄, 𝔅, and ℭ may be added together to yield the total valence-effect EFG. For the component parallel to $\vec{R}$, this is

$$q_{\parallel}^{V} \equiv q_{\parallel}^{\mathfrak{A}} + q_{\parallel}^{\mathfrak{B}} + q_{\parallel}^{\mathfrak{C}} . \tag{14}$$

Because of the cylindrical symmetry of the valence-effect EFG, any EFG component perpendicular to $\vec{R}$ will be equal to $-\frac{1}{2}q_{\parallel}^{V}$. $q_{\parallel}^{\mathfrak{A}}$, $q_{\parallel}^{\mathfrak{B}}$, $q_{\parallel}^{\mathfrak{C}}$, and $q_{\parallel}^{V}$ for *Cu*Cd are shown in Fig. 2.

III. THEORY OF THE SIZE EFFECT

We account for three effects which result from the difference in size between the impurity and host atoms. The first two of them are corrections to the valence-effect calculation, and may therefore be regarded as indirect.

The first indirect size effect is simply that the host atoms in the alloy will occupy positions different from those they would occupy in the ideal lattice; the charge effect EFG's must be evaluated at the new atomic positions which are appropriate to the alloy. Although this effect is elementary, it has been ignored both in previous EFG calculations and in calculations of the spin perturbations about transition-metal and rare-earth impurities.

The second indirect size effect is the Blatt correction.[24] Most calculations of the scattering phase shifts of conduction electrons employ the Friedel sum rule[25]

$$Z_{\text{eff}} = \frac{2}{\pi} \sum_{l} (2l+1)\delta_l ,$$

where δ_l is the phase shift appropriate to electrons having orbital angular momentum with quantum number l, and Z_{eff} is the effective difference in charge between impurity and host ion. In Blatt's method, Z_{eff} is taken to be

$$Z_{\text{eff}} = \left(1 - \frac{3}{\gamma_E} a^{-1} \frac{da}{dc}\right) Z_0 ,$$

where Z_0 is the nominal valence difference, γ_E is a function of the Poisson ratio, equal to 1.44 for Cu, and $a^{-1}(da/dc)$ is the change in lattice parameter per unit concentration of impurity. The Blatt correction changes the scattering phase shifts and thereby modifies the valence-effect contribution to the EFG. All the valence-effect calculations done in this paper used the Hurd-Gordon phase shifts,[26] in which account was taken of the Blatt correction.

The direct contribution of the size-effect EFG, introduced for alloys by SPH, is based on the postulate that the EFG at a lattice site contains a term proportional to the local strain.[5] Béal-Monod and Kohn have shown how both the direct size effect and the Blatt correction can be derived from the theory of the electron gas.[27] Although their theory applies to EFG's far from impurity sites, we shall assume the direct size effect and the Blatt correction are also correct and independent near the impurity.

To calculate the direct size effect (henceforth, simply "the" size effect), we assume the displacement is spherically symmetric about the impurity, and that it can be written

$$\vec{u} = \frac{\vec{r}}{r} \sum_{n=2}^{\infty} \frac{D_n}{r^n} , \tag{15}$$

where the D_n are constants.[28]

The components of the symmetric strain tensor are given by

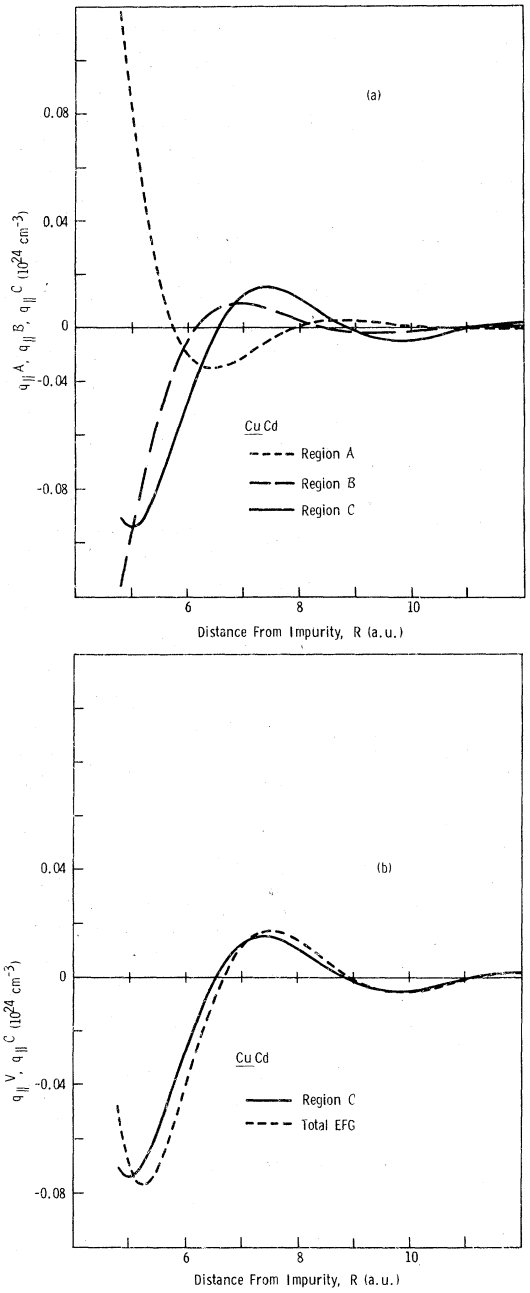

FIG. 2. (a) Comparison of $q_{\parallel}^{\mathfrak{A}}$, $q_{\parallel}^{\mathfrak{B}}$, and $q_{\parallel}^{\mathfrak{C}}$, as function of host-impurity distance in *Cu*Cd. (b) Comparison of $q_{\parallel}^{\mathfrak{C}}$ with the total valence-effect EFG $q_{\parallel}^{V}$ as function of host impurity distance in *Cu*Cd.

$$\epsilon_{ij}=\frac{1}{2}\left(\frac{\partial u_i}{\partial x_j}+\frac{\partial u_j}{\partial x_i}\right), \tag{16}$$

where x_1, x_2, x_3 are Cartesian coordinates. Applying Eq. (16), we find the nth term in Eq. (15) is

$$\begin{aligned}\epsilon_{xx}^{(n)}&=D_n[1/r^{n+1}-x^2(n+1)/r^{n+3}],\\ \epsilon_{xy}^{(n)}&=D_n xy(n+1)/r^{n+3}.\end{aligned} \tag{17}$$

The other components may be obtained by cyclic permutation of x, y, z. Henceforth we assume the xyz system to be parallel to the crystal axes, as shown in Fig. 3.

Referring to Fig. 3, we see that the coordinates of a typical 1NN copper atom are $(0, d_1/\sqrt{2}, d_1/\sqrt{2})$, and that the coordinates of a typical 2NN atom are $(0, 0, d_2)$. In the perfect lattice, $d_1 = a/\sqrt{2}$ and $d_2 = a$, where a is the lattice parameter of pure copper. We will evaluate the strain and the resultant field gradient at the displaced atomic positions, found by using Eq. (15), as was done for the valence effect.

Evaluating Eq. (17) at the 1NN site

$$\begin{aligned}&\epsilon_{xx}^{(n)}=D_n/d_1^{n+1},\quad \epsilon_{yy}^{(n)}=\epsilon_{zz}^{(n)}=-(n-1)D_n/2d_1^{n+1},\\ &\epsilon_{xy}^{(n)}=\epsilon_{zx}^{(n)}=0,\quad \epsilon_{yz}^{(n)}=-(n+1)D_n/4d_1^{n+1},\\ &\sum_i \epsilon_{ii}^{(n)}=(2-n)\frac{D_n}{d_1^{n+1}}.\end{aligned} \tag{18}$$

At the 2NN site

$$\begin{aligned}&\epsilon_{xx}^{(n)}=\epsilon_{yy}^{(n)}=D_n/d_2^{n+1},\quad \epsilon_{zz}^{(n)}=-nD_n/d_2^{n+1},\\ &\epsilon_{xy}^{(n)}=\epsilon_{yz}^{(n)}=\epsilon_{zx}^{(n)}=0,\\ &\sum_i \epsilon_{ii}^{(n)}=(2-n)\frac{D_n}{d_2^{n+1}}.\end{aligned} \tag{19}$$

The correct expression for the components of the traceless EFG tensor q_{ij}^{S}, linear in local strain, is[5]

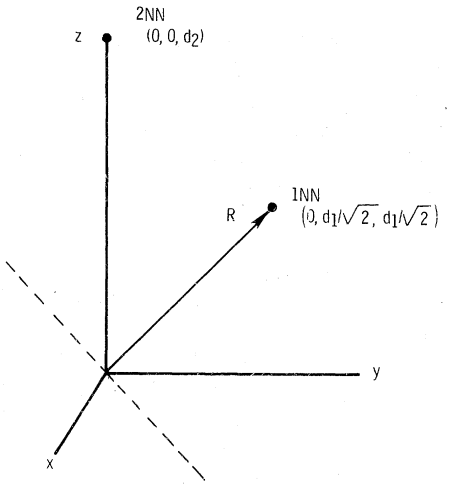

FIG. 3. Crystal coordinate system used in calculation of size effect EFG. Impurity atom is at the origin. d_1 and d_2 are, respectively, the distances from the impurity to the 1NN and 2NN sites. The 1NN host atom is in the yz plane. Lower case letters x, y, z, are used for the crystal coordinates, whereas upper case letters X, Y, Z, are used to label principal axes of the EFG tensor.

$$q_{ij}^S \equiv \frac{1}{e}(V_{ij} - \tfrac{1}{3}\nabla^2 V),$$

$$= \frac{1}{e}\left[(F_{11}-F_{12})\delta_{ij}\left(\epsilon_{ii} - \tfrac{1}{3}\sum_k \epsilon_{kk}\right) + 2(1-\delta_{ij})F_{44}\epsilon_{ij}\right]. \quad (20)$$

The F_{mn} are components of a fourth-order tensor where, in the Voigt notation, $m,n = 1, 2, \ldots, 6$. i,j,k, correspond to the Cartesian coordinates x,y,z.

Substituting Eq. (18) into Eq. (20), we have for the 1NN site

$$q_{xx}^S = (1/3e)G_1(F_{11}-F_{12}),$$
$$q_{yy}^S = q_{zz}^S = -(1/6e)G_1(F_{11}-F_{12}), \quad (21)$$
$$q_{yz}^S = -(1/2e)G_1F_{44}, \quad q_{xy}^S = q_{zx}^S = 0.$$

And substituting Eq. (19) into Eq. (20) we have for the 2NN site

$$q_{xx}^S = q_{yy}^S = (1/3e)G_2(F_{11}-F_{12}),$$
$$q_{zz}^S = -(2/3e)G_2(F_{11}-F_{12}), \quad (22)$$
$$q_{xy}^S = q_{yz}^S = q_{zx}^S = 0.$$

In Eqs. (21) and (22)

$$G_1 = \sum_{n=2}^{\infty} \frac{(n+1)D_n}{d_1^{n+1}}$$

and

$$G_2 = \sum_{n=2}^{\infty} \frac{(n+1)D_n}{d_2^{n+1}}.$$

We must now determine the principal values and the principal axes $\{X,Y,Z\}$ for the size-effect EFG. We note first that at the 2NN site $\vec{q}^{\,S}$ is diagonal, so the crystal coordinate system is a principal-axis system. The asymmetry parameter for the EFG η is defined as[18]

$$\eta \equiv (q_{XX} - q_{YY})/q_{ZZ}. \quad (23)$$

The asymmetry parameter for the 2NN site is seen to be zero (as it must be, since $\vec{R}$ is along a fourfold-symmetry axis). The EFG q_{ZZ}^S is in this case along z, or parallel to $\vec{R}$. Thus at the 2NN site the principal axes of the valence-effect tensor and the size-effect tensor coincide exactly, independent of the values of the $\vec{\vec{F}}$ tensor.

At the 1NN site the tensor $\vec{q}^{\,S}$ is not diagonal in the xyz system. Diagonalizing the tensor in the usual way[29] we find

$$q_{xx}^S = (1/3e)G_1(F_{11}-F_{12}),$$
$$q_{\perp}^S = (1/6e)G_1[-(F_{11}-F_{12}) + 6F_{44}], \quad (24)$$
$$q_{\parallel}^S = (1/6e)G_1[-(F_{11}-F_{12}) - 6F_{44}].$$

The subscripts xx, $\perp$, and $\parallel$ label the principal axes of $\vec{q}^{\,S}$ at the 1NN site. They refer (Fig. 3), respectively, to the x axis of the crystalline system, the axis perpendicular simultaneously to the x axis and the $\vec{R}$ direction, and the axis parallel to the $\vec{R}$ direction—that is, to the [100], [0$\bar{1}$1], and [011] directions.

Since the Z axis for the valence-effect tensor $\vec{q}^{\,V}$ is parallel to $\vec{R}$, the principal-axis systems for $\vec{q}^{\,S}$ and $\vec{q}^{\,V}$ can be made to coincide. However, from Eq. (24) it is clear that the identification of the Z axis for $\vec{q}^{\,S}$ at the 1NN site will depend on the relative values of $(F_{11}-F_{12})$ and F_{44}. In general, therefore, one cannot simply add the values of $q_{\parallel}^S$ and $q_{\parallel}^V$ algebraically at the 1NN site to get the total 1NN EFG.

SPH assumed that $F_{44} = \frac{1}{2}(F_{11}-F_{12})$ in order to simplify the calculation. It is readily verified, using Eq. (24), that this "isotropy condition" gives $\eta = 0$ and makes the Z axis parallel to $\vec{R}$. The q's for the valence and size effects can then be added. SPH found that for calculating wipe-out numbers—which are a kind of average over a large region of the crystal—this was a reasonable approximation.

In this paper we do not use the isotropy condition. We assume instead that the components of the $\vec{\vec{F}}$ tensor are given by the point-charge model[5,30]

$$F_{11} - F_{12} = -3F_{44} = 18\sqrt{2}\,\lambda e/a^3, \quad (25)$$

where, as before, a is the lattice parameter for the unstrained crystal and λ is a dimensionless parameter which relates the experimental EFG to the EFG which would be observed if the distorted lattice were made up of unshielded point charges.[31,32] For host atoms far from the impurities, one would expect λ to be the same for all impurities. However, at the 1NN site, effects due to the electronic structure of the impurity might be important.

Substituting Eq. (25) into (24),

$$q_{xx}^S = 6\sqrt{2}\,\lambda G_1/a^3, \quad q_{\perp}^S = -9\sqrt{2}\,\lambda G_1/a^3,$$
$$q_{\parallel}^S = 3\sqrt{2}\,\lambda G_1/a^3 \quad (26)$$

for the 1NN site in the point-charge model. From this it is clear that the size-effect Z axis is in the perpendicular direction, the Y axis is the crystal x axis, and the X axis is in the parallel direction. As prophesied above, the Z axes of $\vec{q}^{\,V}$ are $\vec{q}^{\,S}$ are not identical.

Equation (26) is *qualitatively* consistent with one of the desired results—a nonzero asymmetry parameter. If local strain were the only source of the EFG, then at the 1NN site η would have the value $\frac{1}{3}$, independent of λ and G_1 (more realistic values of η will be obtained when $\vec{q}^{\,S}$ and $\vec{q}^{\,V}$ are combined).

To complete our analysis of $\tilde{q}^S$ we must determine G_1 and G_2. This requires knowledge of the coefficients D_n. To our knowledge, only D_2 has been treated in detail. Using the misfitting sphere model, one can show[33] that $D_2 = \Delta V/4\pi\gamma_E$, where ΔV is the change in volume per impurity and, as before, $\gamma_E = 1.44$ for copper. If linear isotropic elasticity is assumed with the misfitting sphere model, all other $D_n = 0$. ΔV is related to the fractional change in lattice parameter per unit concentration of impurity $a^{-1}(da/dc)$ through[33]

$$\Delta V = \tfrac{3}{4} a^3 a^{-1} \frac{da}{dc} ,$$

and thus can be determined from x-ray data.[34]

For all the numerical work in this paper we have assumed all $D_n = 0$, except for D_2. Therefore, $G_1 = 3D_2/d_1^3$ and $G_2 = 3D_2/d_2^3$.

Finally we have, at the 1NN site,

$$\begin{aligned} q_{xx}^S &= \frac{54\sqrt{2}}{16\pi\gamma_E} a^{-1} \frac{da}{dc} \lambda d_1^{-3} , \\ q_\perp^S &= -\frac{81\sqrt{2}}{16\pi\gamma_E} a^{-1} \frac{da}{dc} \lambda d_1^{-3} , \\ q_\parallel^S &= \frac{27\sqrt{2}}{16\pi\gamma_E} a^{-1} \frac{da}{dc} \lambda d_1^{-3} \end{aligned} \tag{27}$$

and, at the 2NN site,

$$\begin{aligned} q_\parallel^S &= q_{ZZ}^S = -2q_{XX}^S = -2q_{YY}^S \\ &= -\frac{108\sqrt{2}}{16\pi\gamma_E} a^{-1} \frac{da}{dc} \lambda d_2^{-3} . \end{aligned} \tag{28}$$

IV. COMBINING THE CHARGE AND SIZE EFFECTS

The principal values of the *total* EFG tensor at the 1NN site may now be written

$$\begin{aligned} q_{xx} &= q_{xx}^V + q_{xx}^S = -\tfrac{1}{2} q_\parallel^V + 2q_\parallel^S , \\ q_\perp &= q_\perp^V + q_\perp^S = -\tfrac{1}{2} q_\parallel^V - 3q_\parallel^S , \quad q_\parallel = q_\parallel^V + q_\parallel^S , \end{aligned} \tag{29}$$

where $q_\parallel^V$ is given by Eq. (14) and $q_\parallel^S$ is given by Eq. (27).

The EFG at the 2NN site is given directly by

$$q \equiv q_{ZZ} = q_\parallel^V + q_\parallel^S , \tag{30}$$

where $q_\parallel^S$ is given by Eq. (28).

V. NUMERICAL RESULTS

A. Valence effect

Numerical results for $q_\parallel^V$ are given in Table I for the 1NN and in Table II for the 2NN for alloys containing different dilute impurities in copper. The results were obtained using the Hurd-Gordon phase shifts[26] to determine the parameters A, B, ϕ, ξ in the formulas of Sec. II, and the nuclear quadrupole moment[35]

$$Q(^{63}\mathrm{Cu}) = -0.211 \times 10^{-24} \ \mathrm{cm}^2$$

(this Q differs from values used in Refs. 12–16). The distances at which the EFG's were evaluated are given in the second column of both tables, for each impurity. These distances were evaluated using Eq. (15) with all $D_n = 0$ except D_2. The 1NN contributions from region $\mathfrak{C}$ (Table I) were calculated using the value $\alpha = 15$, and the 2NN contributions (Table II) using the value $\alpha = 18$. These turn out to be the optimum values of α, as discussed below (however, see Sec. V B 2b).

The EFG contributions from regions $\mathfrak{A}$ and $\mathfrak{B}$ are seen generally to have the same order of magnitude as contributions from region $\mathfrak{C}$. Since regions $\mathfrak{A}$ and $\mathfrak{B}$ contribute with opposite signs in all but one case, their net impact is much smaller: $|(q_\parallel^{\mathfrak{A}} + q_\parallel^{\mathfrak{B}})/q_\parallel^{\mathfrak{C}}|_{\mathrm{av}} \simeq \frac{1}{3}$ at both 1NN and 2NN sites.

Tables I and II also contain, for purposes of comparison, the total valence-effect EFG which results if the lattice distortion is neglected, i.e., assuming that the 1NN distance from the impurity is 4.830 a.u., and the 2NN distance is 6.831 a.u. The percentage change in the magnitude of the EFG ranges from near zero to 40%.

In Tables I and II the EFG's are quoted to three significant figures, to match the accuracy of the best experimental results. However, we do not believe the charge density given by Eq. (7) is that accurate at either the 1NN or 2NN sites. At the very least one would like the ratio of preasymptotic to asymptotic terms in the charge density, given by B/Ar, to be small. However, as can be seen from Table III, column 2, such is not the case: If we are to require $|B/Ar| < 0.25$, then in the most favorable case CuGa we would be requiring $r > 16.4$ a.u., i.e., beyond the 12th shell of neighbors.

The contributions of the preasymptotic and asymptotic terms to the charge density and to the EFG also depend greatly on the phase factors ϕ and ξ. In columns 3 and 4 of Table III we give the absolute value of the ratio of the preasymptotic to the asymptotic contributions to the charge density. In columns 5 and 6, and 7 and 8, we give the same ratios for EFG's due to regions $\mathfrak{C}$ and $\mathfrak{A}$, respectively. The average values of the ratios are given at the bottoms of the columns. The preasymptotic term clearly dominates.

We conclude from the results in Table III that the Alfred–Van Ostenburg[20] charge density might not permit accurate calculations of the EFG or charge density at either the 1NN or 2NN site. We have used it in our work, however, because it is the best analytic formula now available.

TABLE III. Comparison of preasymptotic and asymptotic contributions to charge density and to valence-effect EFG in dilute alloys of copper.

		Ratio of magnitude of preasymptotic to asymptotic charge density		Ratio of magnitude of preasymptotic to asymptotic EFG, region $\mathcal{C}$		Ratio of magnitude of preasymptotic to asymptotic EFG, region $\mathcal{A}$	
Impurity	$\lvert B/A\rvert$ [a]	1NN site	2NN site	1NN site	2NN site	1NN site	2NN site
Zn	4.37	1.75	0.88	6.8	1.2	1.8	2.1
Ga	4.10	8.7	1.5	0.68	8.2	0.71	0.33
Ge	4.54	0.54	2.3	0.29	0.77	0.88	0.41
Ag	6.41	0.75	0.25	0.81	0.24	6.3	2.3
Cd	16.4	3.4	1.9	4.0	0.19	24	7.1
In	5.58	4.5	1.4	4.7	2.7	0.47	0.92
Sn	4.60	0.71	19	0.36	1.3	0.82	0.31
Sb	4.57	0.40	0.59	0.03	0.37	1.2	0.51
Avg.		2.5	3.5	2.2	2.1	4.5	1.7

[a] See Eqs. (1) and (7).

B. Valence and size effects combined

1. 2NN sites

The situation at 2NN sites is comparatively simple because of crystal symmetry. There is one experimental datum[36] $|q|$; the Z axis is along $\vec{R}$. In Fig. 4 we plot the "residual EFG," defined as

$$q_{\rm res} \equiv + |q|_{\rm exp} - q_{\parallel}^{V} ,$$

versus the radial component of the strain at the 2NN site. The strain is calculated from Eq. (19) for each impurity. The experimental uncertainties are not well documented in the literature. We have used ± 0.05 Å^{-3} for all the data, as suggested by Nevald.[16] Ga and In are omitted from Fig. 4 because only upper limits for $|q|_{\rm exp}$ are available.

If our theory is correct, $q_{\rm res}$ should lie on a straight line through the origin. This expectation is confirmed by Fig. 4. The straight line shown there is the result of a least-squares fit. The intercept is 0.003 ± 0.03; from the slope and Eq. (28) we find $\lambda = -15 \pm 3$, consistent with the result used by SPH. (In this calculation the value of α was determined by minimizing the standard deviation of λ, and $\alpha = 18$ was found to be optimum.) Our theory is therefore consistent with the 2NN data.

It is interesting that if one uses a negative experimental EFG at the 2NN site, i.e., if one uses $q_{\rm res} \equiv -|q|_{\rm exp} - q_{\parallel}^{V}$, the data points scatter chaotically. Thus our model is consistent with $q > 0$ for the six impurities used for Fig. 4, and with $\lambda < 0$. We will discuss this point in more detail below.

In Table IV we present theoretical results for $q_{\parallel}^{V}$, $q_{\parallel}^{S}$, and for the total EFG q at the 2NN site, obtained by using Eqs. (28) and (30). The values for $q_{\parallel}^{V}$ are taken from Table II, column 6. Experimental values for $|q|$ are presented to facilitate comparison. The values $\alpha = 18$, $\lambda = -15$ were used in obtaining the results in Table IV. These values are consistent with those of Fig. 4, with those of

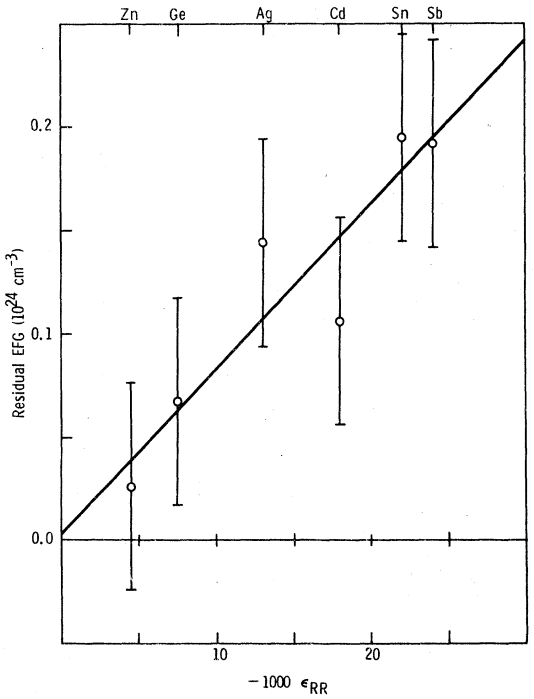

FIG. 4. Residual EFG at the 2NN site as function of the RR component of local strain. *Cu* Ga and *Cu* In have been omitted because only an upper limit to the EFG has been established experimentally. The experimental uncertainty has been taken to be ± 0.05 Å^{-3} (Ref. 16) for all the data. The straight line represents a least-squares fit to the points.

TABLE IV. Theoretical q at 2NN sites in dilute alloys of copper, with $\alpha = 18$, $\lambda = -15$. EFG's are in 10^{24} cm^{-3}.

Impurity	$q^S_{\parallel}$	$q^V_{\parallel}$	q	$\lvert q \rvert_{exp}$	% deviation
Zn	0.037	−0.001	0.035	0.025	41.6
Ga	0.050	0.038	0.088	<0.220	•••
Ge	0.061	0.173	0.234	0.240	−2.5
Ag	0.102	−0.015	0.086	0.129	−33.0
Cd	0.143	0.006	0.149	0.112	33.1
In	0.168	0.029	0.198	<0.120	•••
Sn	0.181	0.121	0.302	0.316	−4.4
Sb	0.193	0.290	0.483	0.482	0.3

SPH, and are within the range of uncertainty KV ascribed to α. The average percent deviation between theoretical and experimental EFG's is 19% (Ga and In are omitted). $q > 0$ is predicted for the 2NN site in all the alloys.

The results for the 2NN sites are only moderately sensitive to the values chosen for α and λ, because of the large experimental uncertainties. From the 2NN data alone, α and λ can be determined to about ±35%. The theoretical ($\alpha = 18$, $\lambda = -15$) and experimental EFG's are plotted in Fig. 5 as a function of nominal valence difference between impurity and host.

2. 1NN sites

a. Alloys with fifth-row impurities. In Table V we present the theoretical predictions for the 1NN EFG's in alloys containing fifth-row impurities. The values (18, −15) for (α, λ), used above for the 2NN data, give good results for the 1NN sites for these alloys. We have chosen, however, to optimize the 1NN results separately by adjusting α and λ. Exact agreement between the 1NN and 2NN values is not to be expected, since α and λ represent asymptotic concepts. The optimum values for the 1NN are (15, −18). It turns out that the theoretical values of η are particularly sensitive to the ratio α/λ, and the new optimum values reduce by a factor of 2 the average magnitude of the percent deviations between theoretical and experimental η's for the fifth-row alloys.

The first row of Table V, under the column headings q_{xx}, $q_{\perp}$, and $q_{\parallel}$, gives the total EFG components for these three principal axes. The second and third rows give separately the size-effect and valence-effect contributions for the same components. The component having the largest magnitude of those in the first row is underlined. It is, by definition, the theoretical EFG q, and its value is listed again the column 6 of Table V. The experimental EFG and the percent deviation are given next. The agreement is very good, except possibly for *Cu*Sb.

From scanning the underlined entries in the first row of Table V, one can see how the Z axis is predicted to vary as a function of impurity. The theory predicts the Z axis to be in the per-

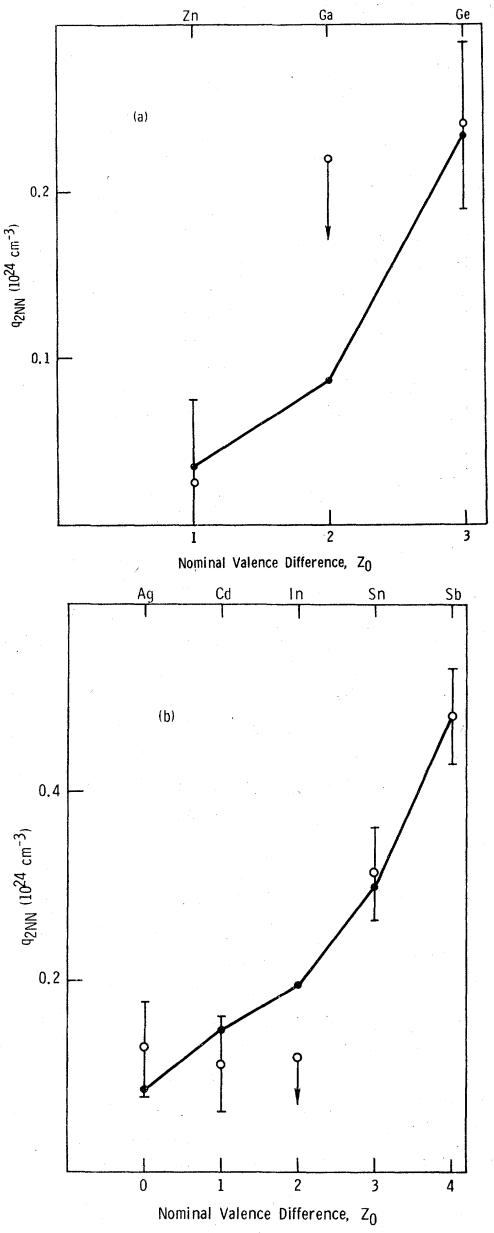

FIG. 5. Experimental (open circles) and theoretical (straight lines) EFG's at the 2NN sites for (a) dilute alloys of copper with impurities from the fourth row of the Periodic Table; (b) dilute alloys of copper with fifth-row impurities. The data are plotted as a function of the nominal host impurity valence difference. Experimental uncertainties are taken to be ±0.05 Å^{-3} (Ref. 16). Vertical arrows for *Cu*Ga and *Cu*In indicate that only upper limits have been experimentally determined. The theoretical results are from Table IV.

TABLE V. Theoretical q and η at 1NN to fifth-row impurites in dilute alloys of copper, with $\alpha = 15$, $\lambda = -18$. EFG's are in 10^{24} cm^{-3}. The contributions of the valence and size effects, and the principal values of the total EFG tensor are also given.[a]

Impurity	EFG contribution	q_{xx}	$q_\perp$	$q_\parallel$	q	$\lvert q\rvert_{exp}$	% deviation, $\lvert q\rvert$	η	η_{exp}	% deviation, η
Ag	Total	−0.186	0.231	−0.045	0.231	0.158	46	0.611	0.725	−16
	Size	−0.167	0.250	−0.083						
	Valence	−0.019	−0.019	0.038						
Cd	Total	−0.211	0.367	−0.157	0.367	0.414	−11	0.148	0.036	311
	Size	−0.231	0.347	−0.116						
	Valence	0.020	0.020	−0.041						
In	Total	−0.172	0.501	−0.329	0.501	0.607	−17	0.313	0.320	−2
	Size	−0.270	0.404	−0.135						
	Valence	0.097	0.097	−0.194						
Sn	Total	−0.049	0.672	−0.623	0.672	0.632	6	0.854	0.630	36
	Size	−0.288	0.433	−0.144						
	Valence	0.239	0.239	−0.479						
Sb	Total	0.137	0.905	−1.042	−1.042	0.719	45	0.736	0.740	−1
	Size	−0.307	0.460	−0.153						
	Valence	0.444	0.444	−0.888						

[a] Because of rounding off, the EFG's may not appear to be exactly traceless in all cases.

pendicular direction (EFG dominated by the size effect) for the Ag, Cd, In, and Sn alloys, and to be in the parallel direction (EFG dominated by the valence effect) for the Sb alloy. The NMR experiments[13-15] have been able to establish that the Z axis is either in the perpendicular or parallel direction (they cannot discriminate between the two directions), and our results are therefore consistent with experiment. The theoretical q's are positive for the Ag, Cd, In, and Sn alloys, and negative for the Sb alloy; as mentioned earlier, the NMR experiments can determine $|q|$ but not its sign.[36]

Theoretical and experimental q's are plotted versus nominal valence difference in Fig. 6(a). The signs of the experimental EFG's have been chosen to agree with the theory. The fit is good, except possibly for the overshoot at *Cu*Sb. It is interesting that if we had used the perfect lattice value for the 1NN distance for *Cu*Sb we would have obtained $q = -1.20$ Å^{-3}, instead of the $q = -1.04$ Å^{-3} obtained in the distorted lattice. Using the corrected lattice parameters produces in this case a significant improvement in agreement between theory and experiment.

In columns 9–11 of Table V we give theoretical and experimental asymmetry parameters, and percent deviation. The results are plotted versus nominal valence difference in Fig. 6(b). The prediction of the large dip in the value of η for *Cu*Cd is a striking success for the theory. (The large percent deviation in that case can be understood in terms of the sensitivity of η to the ratio α/λ, mentioned above. $\alpha = 22$, $\lambda = -18$ give values of q and η which agree to within experimental uncertainty with the *Cu*Cd data.)

The 1NN data can also be fitted with a different set of parameters—$\alpha = -18$, $\lambda = +15$. We disregard this result, since calculations have consistently resulted in $\alpha > 0$ (the only exceptions known to us are calculations by Fukai for Pb-based alloys[37]). The result $(-18, +15)$ arises in the theory because we cannot specify the sign of q.[36] If only region ℭ were to be considered in the valence-effect calculation, then a change in the signs of *both* α and λ would leave $|q|$ and η unaffected. Thus to every solution (α, λ) that is consistent with experiment there would be a corresponding solution $(-\alpha, -\lambda)$. Inclusion of regions 𝔄 and 𝔅 in the valence-effect changes quantitative details, since the EFG's arising from those regions depend on $(1 - \gamma_\infty)$ rather than on α, but it does not alter the basic picture sketched. (Incidentally, changing the signs of both α and λ does not affect the conclusion of SPH because the second-order interaction studied by them depends upon q^2.)

b. Alloys with fourth-row impurities. Theoretical results with $\alpha \simeq +18$, $\lambda \simeq -15$ fail completely to reproduce the experimental 1NN data for *Cu*Zn, *Cu*Ga, and *Cu*Ge. However, using the empirical equations of Appendix B, we have found there is a single (α, λ) region surrounding $\alpha = +2$, $\lambda = +87$ for which all the experimental data can be fit. The values of q and η corresponding to $(+2, +87)$ are given in Table VI, and are plotted versus nominal host impurity valence difference in Fig. 7.

The agreement between theory and experiment is remarkable. The average deviation between

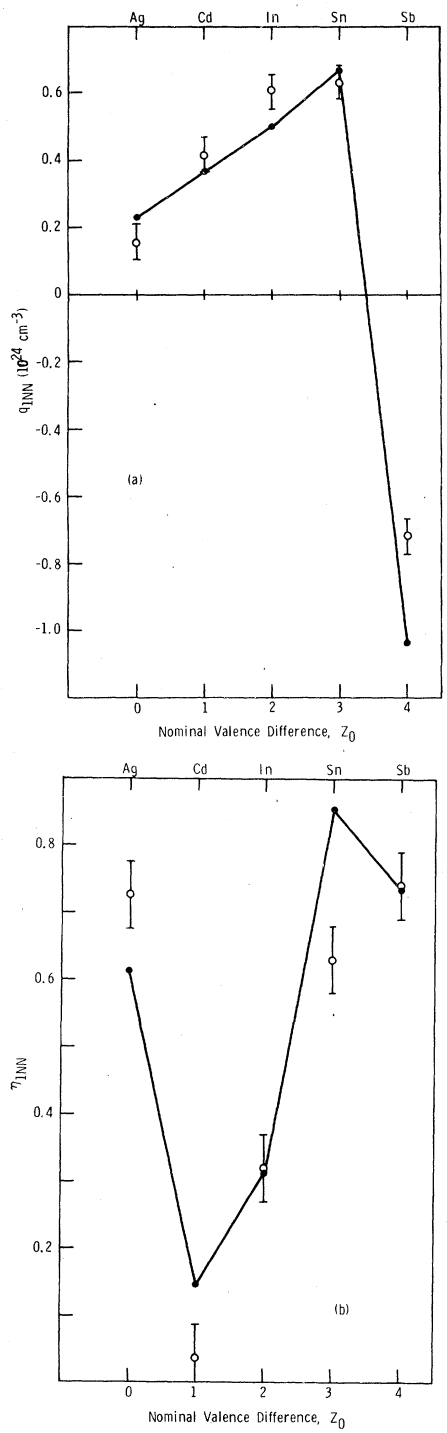

FIG. 6. Experimental (open circles) and theoretical (straight lines) 1NN EFG parameters, as function of nominal host impurity valence difference, for dilute alloys of copper with impurities from the fifth row of the Periodic Table. (a) EFG parameter q; (b) asymmetry parameter η. Experimental uncertainties are taken to be ± 0.05 Å^{-3} for q, and ± 0.05 for η (Ref. 16). Theoretical results are from Table V.

theoretical and experimental q's is 13%, and the average deviation between the η's is 10%. These average deviations are smaller than the experimental uncertainties.

Even more striking is the successful prediction of the anomalous direction of the Principal Axis for *Cu*Ge. When the values (2, 87) are used, the theory correctly predicts that the Principal Axis of the 1NN EFG lies along the crystalline [100], or x, direction.

Examination of the separate size- and valence-effect contributions to the EFG (see Table VI) reveals that the anomalous direction of the 1NN EFG in *Cu*Ge results from an interference effect. In the parallel and perpendicular directions the valence and size contributions tend to cancel because they are of comparable magnitude but of opposite sign. However, the valence and strain contributions have the *same* sign in the [100] direction.

In *Cu*Zn and *Cu*Ga the EFG's are dominated by the size effect, and the Principal Axis is in the perpendicular direction, consistent with experiment.

The predictions for fourth row alloys are very sensitive to the value of λ, which can be determined from the data to about $\pm 15\%$. However, the percentage accuracy of the value $\alpha = 2$ is quite poor because when α has such a low value the valence effect is dominated by regions Ⓐ and Ⓑ. We remark, finally, that the parameters (2, 87) give very poor results for all the 2NN data, and for the fifth-row impurity 1NN data.

VI. DISCUSSION

Our calculations, using values of the parameter α and λ which are consistent with the $\alpha = 23.3$ of KV (who estimated their calculation to be good to within a factor of 2) and the $\lambda = -15$ of SPH, are in good agreement with all the 2NN data and with the 1NN data for alloys with fifth-row impurities. For the 2NN data the optimum values of the parameters are (18, −15); and for the 1NN fifth-row data (15, −18).

On the other hand, agreement with the 1NN fourth-row data can be obtained only with $\alpha = 2$, $\lambda = 87$, and for no other range of values of the parameters. The physical significance, if any, of this tremendous discrepancy in (α, λ) values is not at all clear to us. We have, with only two adjustable parameters, been able to account for nine pieces of experimental data—$|q|$, η, and the direction of the Principal Axis, for three fourth-row alloys. It is tempting to argue that this is unlikely to be accidental, and to ascribe physical significance to these particular values of α and λ. However, it is conceivable that the 1NN fourth-row re-

TABLE VI. Theoretical q and η at 1NN to fourth-row impurities in dilute alloys of copper, with $\alpha = 2$, $\lambda = 87$. EFG's are in 10^{24} cm^{-3}. The contributions of the valence and size effects, and the principal values of the total EFG tensor are also given. [a]

Impurity	EFG contribution	q_{xx}	$q_\perp$	$q_\parallel$	q	$\lvert q\rvert_{exp}$	% deviation $\lvert q\rvert$	η	η_{exp}	% deviation η
Zn	Total	0.295	−0.445	0.150	−0.445	0.534	−17	0.324	0.265	22
	Size	0.296	−0.444	0.148						
	Valence	−0.001	−0.001	0.003						
Ga	Total	0.438	−0.563	0.125	−0.563	0.599	−6	0.555	0.590	−6
	Size	0.401	−0.601	0.200						
	Valence	0.037	0.037	−0.075						
Ge	Total	0.622	−0.599	−0.022	0.622	0.528	18	0.928	0.905	3
	Size	0.488	−0.733	0.244						
	Valence	0.133	0.133	−0.267						

[a] Because of rounding-off, the EFG's may not appear to be exactly traceless in all cases.

sults are fortuitous. There are, after all, eight (α, λ) pairs which can be made to agree exactly with experiment for *Cu*Zn, another eight for *Cu*Ga, and four for *Cu*Ge (see Appendix B). We may be seeing an accidental overlap of three incorrect (α, λ) pairs.

It should be emphasized—cf. Appendix B—that the large number of (α, λ) pairs results from the fact that the 1NN EFG tensor is incompletely characterized by the NMR experiment. We do not know the directions of all the principal axes in the XYZ system, and we do not know the sign of q. If complete experimental information were available, there would be only one pair (α, λ) for each impurity, which would account for the experimental results. Of course, if we had to use radically different values for each impurity, we would be inclined to doubt the physical significance of the model, with the caveat that at the 1NN things may be very complicated.

Using Appendix B one can find (α, λ) solutions for Zn and Ga which at least have the same signs as the 2NN values and which differ in magnitude by no more than a factor of 5—for example, (60,

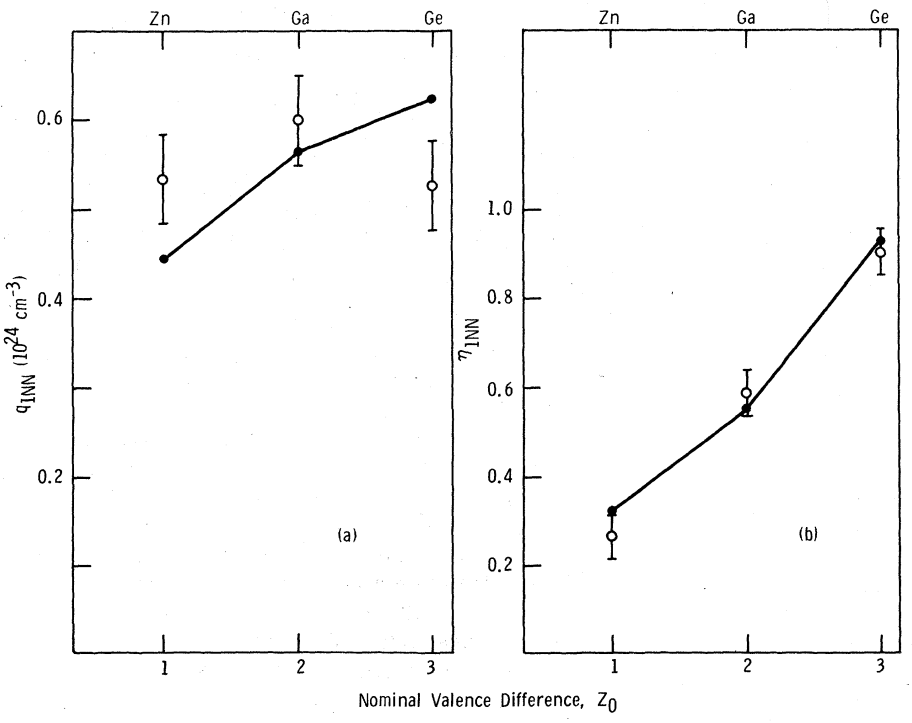

FIG. 7. Experimental (open circles) and theoretical (straight lines) 1NN EFG parameters, as function of nominal host impurity valence difference, for dilute alloys of copper with impurities from the fourth row of the Periodic Table. (a) EFG parameter q; (b) asymmetry parameter η. Experimental uncertainties are taken to be ± 0.05 Å^{-3} for q, and ± 0.05 for η (Ref. 16). Theoretical results are from Table VI.

−84) for *Cu*Zn and (26, −61) for *Cu*Ga. However, *Cu*Ge is completely anomalous because of the direction of the Principal Axis. In every case the allowed values of α and λ have the same sign. *Cu*Si is also known experimentally to have the 1NN Principal Axis in the x direction. We could not calculate the allowed values of α in this case because the Hurd-Gordon phase shifts are not available. However, the only allowed values of λ for *Cu*Si are 228 and 377, indicating that *Cu*Si is probably more anomalous than *Cu*Ge. We may be seeing manifestations of the unique chemical properties of Ge and Si.

Even within the context of the present model, the theory could be considerably improved. The principal shortcoming of the valence-effect calculation is the domination, at host sites near the impurity, of the preasymptotic term in the screening charge. This domination over the asymptotic term does not encourage hope that progress will result simply through adding more terms to the expansion. An entirely new method probably will be needed. There is also strong evidence that the displacements and strains predicted by Eqs. (15)–(19) are inaccurate close to the impurity. Flinn and Maradudin, using a lattice calculation, have shown that the elastic-continuum model we employ considerably underestimates the displacements at the 1NN site.[38] Since that work did not include calculations of the strain, we were unable to incorporate the findings into our model. Townsend has extended the elastic-continuum model by using more realistic forces, but has applied his formalism only to vacancy effects.[39]

An improved calculation for α would also be desirable. The KV calculation is valid only in the asymptotic limit, and does not account for the directionality of α.[40] Also, for a more detailed check on our theory, knowledge of the sign of q would be desirable.

The values of λ required in this work to interpret the experimental data, and in SPH as well, are much larger than the $|\lambda| < 2$ which was determined from plastically deformed copper.[6–9] We have reexamined the experiments on plastically deformed copper, accounting for the fact that plastic deformation introduces dislocations and dislocation structures.[32] We believe the low value of $|\lambda|$ obtained by Averbuch *et al.*[6] results from use of an oversimplified model (uniform strain) of the defect structure, and that the low value in the case of the Faulkner experiment[7] (as interpreted by Ogurtani and Huggins[8,9]) results from an overestimate of the stored elastic energy. Our simple calculations, using dislocation monopoles and dipoles, indicate the Averbuch and Faulkner experiments are consistent with $|\lambda| > 10$.[32]

VII. SUMMARY AND CONCLUSIONS

In this paper we have interpreted the measurements of the EFG and asymmetry parameter at host atoms which are near isolated fourth- and fifth-row non-transition-metal impurities in copper-based alloys. Our most important conclusion is that the experimental data can be understood if account is taken of size effects which arise because the impurity atom distorts the host crystalline lattice.

By using a point-charge model for the EFG due to the direct size effect (lowering of the local symmetry about the host atom), and by adding its tensor components to the well-known valence-effect EFG, we have obtained quantitative agreement with the experimental values of $|q|$ and η, and the directions of the Principal Axes of the EFG tensors. The values of the core enhancement factor α and the EFG-strain coupling constant λ, obtained for all of the 2NN EFG's and for the 1NN EFG's of alloys with fifth-row impurities (*Cu*Ag, *Cu*Cd, *Cu*In, *Cu*Sn, and *Cu*Sb), are consistent both among themselves and with the work of Kohn and Vosko, and of Sagalyn, Paskin, and Harrison. The values of α and λ required for the 1NN EFG's of the alloys with fourth row impurities (*Cu*Zn, *Cu*Ga, and *Cu*Ge), however, are anomalous; the physical significance, if any, of the parameters for these alloys is not clear.

We have also improved the calculation of the valence-effect EFG. We have explicitly calculated the contribution of the screening charge which is outside the host atom sphere. Asymptotically this contribution is about 17% of the contribution from within the host sphere (assuming $\alpha = 23.3$)—confirming the original estimate of Kohn and Vosko—but the contribution can be considerably larger when the host atoms are near neighbors of the impurity. Our valence effect calculations have, also, accounted for the fact that in the alloy host atoms are displaced from the perfect crystal lattice positions. The correction, while elementary, is not negligible.

ACKNOWLEDGMENTS

We thank Dr. R. J. Harrison for discussing several aspects of this work with us, and for his perceptive remarks about the manuscript. Correspondence with Professor R. Nevald on his work is acknowledged.

APPENDIX A: ASYMPTOTIC FORM OF $q_{\parallel}^{\otimes}$

The EFG at a host site due to the screening charge outside the atomic sphere is [cf. Eqs. (7), (13)]

$$q_{\parallel} = \begin{cases} -2(1-\gamma_\infty)\int r'^{-3} P_2(\cos\theta')[Ar^{-3}\cos(Kr+\phi) \\ \qquad + Br^{-4}\cos(Kr+\xi)]\, dV, & \text{(A1)} \\ -2(1-\gamma_\infty)(A\mathcal{I}_1 + B\mathcal{I}_2)\,, & \text{(A1')} \end{cases}$$

where $K = 2k_F$, $\{r, \theta, \Phi\}$ are the spherical coordinates of volume element dV in a system centered at the impurity, and $\{r', \theta', \Phi'\}$ are the spherical coordinates of the volume element in a system centered at the host atom. The host and impurity atoms are separated by a distance R.

The expression above contains a mixture of the two coordinate systems. We use the following transformation from the impurity-centered system to the host-centered system[41]:

$$(Kr)^{-1}e^{iKr} = i\sum_{n=0}^{\infty}(2n+1)P_n(\cos\theta') \times j_n(Kr')h_n(KR)\,, \qquad \text{(A2)}$$

where P_n is the Legendre polynomial of order n, j_n is the spherical Bessel function of order n, $h_n = j_n + in_n$, and n_n is the spherical Neumann function of order n. Equation (A2) holds if $r' < R$; interchange of r' and R permits use of the formula when $r' > R$.

We illustrate the use of Eq. (A2) by considering the integral

$$\mathcal{I}_1 = \int P_2(\cos\theta')r'^{-3}r^{-3}\cos(Kr+\phi)\, d^3r'\,. \qquad \text{(A3)}$$

For large R, $r \simeq R$ in region ℬ (see Fig. 1). Thus, r^{-2} will vary much more slowly than $\cos(Kr+\phi)$ in the integration over region ℬ, and we write

$$\mathcal{I}_1 \simeq KR^{-2}\int P_2(\cos\theta')r'^{-3}(Kr)^{-1} \times(\cos Kr\cos\phi - \sin Kr\sin\phi)\, d^3r'\,. \qquad \text{(A4)}$$

We now substitute for $(Kr)^{-1}\sin Kr$ and $(Kr)^{-1}\cos Kr$ the expressions obtained from the real and imaginary parts of Eq. (A2). The result simplifies greatly if we can exploit the orthogonality of the P_n, for then only the terms in P_2 contribute to $\mathcal{I}_1$. We therefore extend the integral over all space except for the sphere of radius $\frac{1}{2}d$ which is centered on the host atom (i.e., region ℭ). Since, as was pointed out in Sec. II of the main text, there is no net EFG due to screening charge outside the sphere of radius $R+\frac{1}{2}d$ in Fig. 1, the integral $\mathcal{I}_1$ now measures contributions from regions 𝔄 and ℬ. The contribution of region 𝔄 will be subtracted out after we complete the outline of how $\mathcal{I}_1$ and $\mathcal{I}_2$ are computed.

Thus, using the orthogonality relation for the P_n,[42] we have

$$\mathcal{I}_1 \simeq -4\pi KR^{-2}\left(\cos\phi\, n_2(KR)\int_{d/2}^{R} r'^{-1}j_2(Kr')\,dr' + \cos\phi\, j_2(KR)\int_R^{\infty} r'^{-1}n_2(Kr')\,dr' + \sin\phi\, j_2(KR)\int_{d/2}^{\infty} r'^{-1}j_2(Kr')\,dr'\right). \qquad \text{(A5)}$$

Equation (A5) is evaluated by using the indefinite integral

$$\int z^{1-n}f_n(z)\,dz = -z^{1-n}f_{n-1}(z)\,, \qquad \text{(A6)}$$

where $f_n(z) = aj_n(z) + bn_n(z)$, and a and b depend neither on z nor on n.[41] Thus $\mathcal{I}_1$ has been reduced to a sum of j_1, n_1, j_2, and n_2. We substitute their functional forms[43] to obtain the final result.

The same techniques are applied to the $\cos(Kr+\xi)$ term in Eq. (A1) to evaluate $\mathcal{I}_2$. Then, using Eq. (A1') we have the EFG.

We write the "EFG" so determined as $\tilde{q}_{\parallel}^{\mathfrak{A}} + q_{\parallel}^{\mathfrak{B}}$. As discussed above, the "EFG" consists of a valid approximation to $q_{\parallel}^{\mathfrak{B}}$, plus a contribution from region 𝔄 which arose because the integration was extended over all space. We now evaluate $\tilde{q}_{\parallel}^{\mathfrak{A}}$.

The evaluation of $\tilde{q}_{\parallel}^{\mathfrak{A}}$ is based on the observation that in making the transition from Eq. (A3) to Eq. (A4) we were, from a physical point of view, changing the expression for the screening charge density. The charge density we used was (to lowest order in $1/R$)

$$\Delta\tilde{n}(r) = -AR^{-2}r^{-1}\cos(Kr+\phi)\,. \qquad \text{(A7)}$$

The tilde indicates the charge density is artificial, as it is approximately correct only in region ℬ in the limit of large R. However, if we compute the total "charge" $\tilde{Q}$ corresponding to $\Delta\tilde{n}$ which is enclosed in region 𝔄, we know $\tilde{q}_{\parallel}^{\mathfrak{A}}$ through Gauss's law

$$e\tilde{q}_{\parallel}^{\mathfrak{A}} = -2\tilde{Q}(1-\gamma_\infty)R^{-3}. \qquad \text{(A8)}$$

The calculation is straightforward. Integrating Eq. (A7) over region 𝔄,

$$\tilde{Q} = -4\pi AR^{-2}e\int_0^{R-d/2}(\cos Kr\cos\phi - \sin Kr\sin\phi)r\,dr$$

$$\sim -4\pi AK^{-1}R^{-1}e\left[\sin\tfrac{1}{2}Kd\cos(KR+\phi) - \cos\tfrac{1}{2}Kd\sin(KR+\phi)\right].$$

Therefore,

$$\tilde{q}_{\parallel}^{\mathfrak{G}} \sim 8\pi A(1-\gamma_\infty)K^{-1}R^{-4}[\sin\tfrac{1}{2}Kd\cos(KR+\phi) - \cos\tfrac{1}{2}Kd\sin(KR+\varphi)]\,. \tag{A9}$$

This is subtracted from the result we derived for $-2(1-\gamma_\infty)(A\mathfrak{g}_1+B\mathfrak{g}_2)$.

The final result for the asymptotic form for $q_{\parallel}^{\mathfrak{G}}$, good to order R^{-4}, is thus

$$q_{\parallel}^{\mathfrak{G}} \sim C_0 R^{-3}\cos(2k_F R+\phi) + R^{-4}[C_1\sin(2k_F R+\phi) + C_2\cos(2k_F R+\phi)+C_3\cos(2k_F R+\xi)]\,, \tag{A10}$$

where

$$C_0 = 8\pi A(1-\gamma_\infty)[(k_F d)^{-3}\sin k_F d - (k_F d)^{-2}\cos k_F d]\,,$$
$$C_1 = 4\pi A(1-\gamma_\infty)k_F^{-1}\{[3(k_F d)^{-2}-1]\cos k_F d - 3(k_F d)^{-3}\sin k_F d\}\,,$$
$$C_2 = 4\pi A(1-\gamma_\infty)k_F^{-1}\sin k_F d\,,$$
$$C_3 = 8\pi B(1-\gamma_\infty)[(k_F d)^{-3}\sin k_F d - (k_F d)^{-2}\cos k_F d]\,.$$

APPENDIX B: EQUATIONS FOR $\vec{q}^{\,V}$ AND $\vec{q}^{\,S}$ IN TERMS OF EXPERIMENTAL q, η, AND DIRECTION OF THE PRINCIPAL AXIS OF THE EFG TENSOR AT THE 1NN

For a given α and λ, the theoretical results summarized in Eq. (29) completely specify the EFG at the 1NN site. That is, they predict the directions of all the principal axes, the sign and magnitude of q, and the value of the asymmetry parameter η. However, we have experimental measurements only of the magnitude of q, and the value of η, plus some incomplete information about the directions of the principal axes. Therefore, if one wishes to determine α and λ in terms of the experimental results, assumptions must be made about the directions of the principal axes and the sign of the gradient.

(i) Assume $\vec{Z}\|\vec{R}$: Using Eq. (29) we can write

$$q_{\parallel} = q_{\parallel}^{V} + q_{\parallel}^{S} = \pm|q|_{\rm exp}\,. \tag{B1}$$

The $\pm$ sign on $|q|_{\rm exp}$ indicates that in principle we can use either sign for making an empirical determination of α and λ.[36] For case (i) we write

$$\pm\eta \equiv (q_{xx}-q_\perp)/q_{\parallel} = 5q_{\parallel}^{S}/\pm|q|_{\rm exp}\,, \tag{B2}$$

substituting from Eqs. (29) and (B1). The ambiguity in the sign of η results from the fact that, given the direction of the Z axis, there are two ways to associate the X and Y directions with the remaining principal axes. Choosing the plus sign for η, for example, means that we require $|q_{xx}| \leq |q_\perp|$, in order that Eq. (A2) be compatible with the definition of η given in Eq. (23).

Solving Eqs. (B1) and (B2) gives

$$q_{\parallel}^{S} = \tfrac{1}{5}[(\pm\eta)(\pm|q|_{\rm exp})] \tag{B3}$$

and

$$q_{\parallel}^{V} = \tfrac{1}{5}\{(\pm|q|_{\rm exp})[5-(\pm\eta_{\rm exp})]\}\,. \tag{B4}$$

Given $q_{\parallel}^{S}$ and $q_{\parallel}^{V}$, λ can be found from the last of Eqs. (27) and α can be found using Eqs. (14) and (1).

In a similiar way we find for the other two possible directions for the Z axis [cases (ii) and (iii), respectively]

$$\vec{Z}\perp\vec{R}\text{:}\quad (\pm\eta_{\rm exp}) \equiv (q_{\parallel}-q_{xx})/q_\perp\,, \tag{B5}$$
$$q_{\parallel}^{S} = \tfrac{1}{10}\{-(\pm|q|_{\rm exp})[3+(\pm\eta_{\rm exp})]\}\,, \tag{B6}$$
$$q_{\parallel}^{V} = \tfrac{1}{5}\{(\pm|q|_{\rm exp})[3(\pm\eta_{\rm exp}-1)]\}\,. \tag{B7}$$
$$\vec{Z}\|\vec{x}\text{:}\quad (\pm\eta) \equiv (q_\perp - q_{\parallel})/q_{xx}\,, \tag{B8}$$
$$q_{\parallel}^{S} = \tfrac{1}{10}\{(\pm|q|_{\rm exp})[3-(\pm\eta_{\rm exp})]\}\,, \tag{B9}$$
$$q_{\parallel}^{V} = \tfrac{1}{5}\{-(\pm|q|_{\rm exp})[2(\pm\eta_{\rm exp})+4]\}\,. \tag{B10}$$

For all the impurities treated in this paper, except germanium, there are eight possible solution pairs (α,λ) to the above equations, corresponding to two possible choices for the Z axis (parallel to $\vec{R}$, or perpendicular to $\vec{R}$ and x), two for the sign of $|q|_{\rm exp}$, and two for the sign of η. For Ge there are only four solutions since the Z axis is known to be parallel to x. If the model used for the sources of the EFG were exact there would be at least one pair of values (α,λ) common to all impurities and consistent with the experimental data. (There might be more than one pair since the experimental information is not complete.) What we actually find are regions of consistency in which the various (α,λ) values are relatively close together. As discussed in the text, for the fifth-row impurities, the only region of consistency for positive α is close to the point $(18,-15)$, and for the fourth-row impurities the only consistent region is in the vicinity of $(+2,+87)$. The empirical equations were particularly useful for finding the latter value pair which is rather remote from the values $(23.3,-15)$ used by SPH.

[1]N. Bloembergen and T. J. Rowland, Acta Metall. 1, 731 (1953).
[2]T. J. Rowland, Phys. Rev. 119, 900 (1960).
[3]W. Kohn and S. H. Vosko, Phys. Rev. 119, 912 (1960).
[4]A. Blandin and J. Friedel, J. Phys. Chem. Solids 17, 170 (1960); A. Blandin and J. Friedel, J. Phys. Radium (Paris) 21, 689 (1960).
[5]P. L. Sagalyn, A. Paskin, and R. J. Harrison, Phys.

Rev. 124, 428 (1961).
[6]P. Averbuch, F. de Bergevin, and W. Müller-Warmuth, C. R. Acad. Sci. (Paris) 249, 2315 (1959).
[7]E. A. Faulkner, Philos. Mag. 5, 843 (1960).
[8]T. O. Ogurtani and R. A. Huggins, Phys. Rev. 137, A1736 (1965).
[9]T. O. Ogurtani and R. A. Huggins, METU J. Pure Appl. Sci. (Ankara, Turkey) 1, 155 (1968).
[10]J. Winter, *Magnetic Resonance in Metals* (Oxford University, New York, 1971), p. 105 ff.
[11]P. L. Sagalyn and J. A. Hofmann, Phys. Rev. 127, 68 (1962); E. P. Jones and D. L. Williams, Phys. Lett. 1, 109 (1962).
[12]A. G. Redfield, Phys. Rev. 130, 589 (1963).
[13]G. Schnakenberg, Jr. and R. T. Schumacher, Phys. Rev. B 7, 2292 (1973).
[14]B. L. Jensen, R. Nevald, and D. L. Williams, J. Phys. F 2, 169 (1972).
[15]R. Nevald, B. L. Jensen, and P. B. Fynbo, J. Phys. F 4, 1320 (1974).
[16]R. Nevald, J. Phys. F 5, L181 (1975).
[17]References on studies of copper-based alloys containing transition-metal impurities, using NMR techniques, may be located by working backward from J. B. Boyce and C. P. Slichter, Phys. Rev. B 13, 379 (1976); D. M. Follstaedt, D. Abbas, T. S. Stakelon, and C. P. Slichter, *ibid.* 14, 47 (1976); and R. Nevald and G. Petersen, J. Phys. F 5, 1778 (1975).
[18]C. P. Slichter, *Principles of Magnetic Resonance* (Harper and Row, New York, 1963), Chap. 6.
[19]The sign of Eq. (8) in Ref. 14 is incorrect. The wrong sign for this equation apparently was also used in Ref. 13. There is also an error in line 2 of p. 177, Ref. 14, as pointed out in Ref. 15.
[20]L. C. R. Alfred and D. O. Van Ostenburg, Phys. Lett. A 26, 27 (1969).
[21]R. M. Sternheimer, Phys. Rev. 84, 244 (1951). We use for γ_∞ the value −17.37, calculated by F. D. Feiock and W. R. Johnson, *ibid.* 187, 39 (1969).
[22]M. Abramowitz and T. A. Stegun, *Handbook of Mathematical Functions*, Natl. Bur. Stands. Appl. Math. Series No. 55 (U.S. GPO, Washington, D. C., 1964), pp. 231–233.
[23]R. J. Harrison and A. Paskin [J. Phys. Soc. Jpn. 15, 1902 (1960)] obtained substantially the same result from dielectric screening theory. See also L. C. R. Alfred, Phys. Lett. A 31, 108 (1970).
[24]F. J. Blatt, Phys. Rev. 108, 285 (1957).
[25]J. Friedel, Adv. Phys. 3, 446 (1954).
[26]C. M. Hurd and E. M. Gordon, J. Phys. Chem. Solids 29, 2205 (1968).
[27]M. T. Béal-Monod and W. Kohn, J. Phys. Chem. Solids 29, 1877 (1968).
[28]Compare with Eqs. (2.3) and (2.4) in P. W. Anderson and S. T. Chui, Phys. Rev. B 9, 3229 (1974).
[29]J. F. Nye, *Physical Properties of Crystals* (Oxford University, New York, 1957), Chap. 2.
[30]E. A. Faulkner, Nature 184, 442 (1959).
[31]N. Bloembergen, *Report of the Conference on Defects in Crystalline Solids* (Physical Society, London, 1955).
[32]M. N. Alexander and P. L. Sagalyn (unpublished).
[33]J. D. Eshelby, Solid State Phys. 3, 79 (1956).
[34]W. B. Pearson, *Lattice Spacings and Structures of Metals and Alloys* (Pergamon, New York, 1958).
[35]R. M. Sternheimer, Phys. Rev. 164, 10 (1967). We have taken $Q(^{63}\mathrm{Cu})$ from G. H. Fuller, J. Phys. Chem. Ref. Data 5, 835 (1976). We thank Dr. Fuller and Dr. G. C. Carter for advice, prior to publication of Dr. Fuller's article, on the choice of $Q(^{63}\mathrm{Cu})$.
[36]Ordinarily only the absolute value of q can be determined by NMR; see A. Abragam, *Principles of Nuclear Magnetism* (Oxford University, London, 1961), p. 261 ff. The sign of the EFG can be determined at sufficiently low temperatures; see A. Abragam and M. Chapellier, Phys. Lett. 11, 207 (1964).
[37]Y. Fukai, Solid State Commun. 9, 1117 (1971); Y. Fukai, J. Phys. (Paris) 33, C3-235 (1972).
[38]P. A. Flinn and A. A. Maradudin, Ann. Phys. (N.Y.) 18, 81 (1962).
[39]J. R. Townsend, Phys. Rev. B 9, 4000 (1974).
[40]See, e.g., P. M. Holtham and P. Jena, J. Phys. F 5, 1649 (1975).
[41]P. M. Morse and H. Feshbach, *Methods of Theoretical Physics* (McGraw-Hill, New York, 1953), p. 1574.
[42]P. M. Morse and H. Feshbach, Ref. 41, p. 1326.
[43]P. M. Morse and H. Feshbach, Ref. 41, p. 1573.